

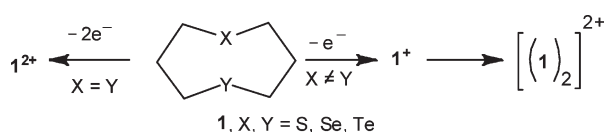
Electrochemical and Chemical Oxidation of Dithia-, Diselena-, Ditellura-, Selenathia-, and Tellurathiamescycles and Stability of the Oxidized Species

Dennis H. Evans,^{*,†} Nadine E. Gruhn,[†] Jin Jin,[‡] Bo Li,[‡] Edward Lorange,[§] Noriko Okumura,[†] Norma A. Macías-Ruvalcaba,[†] Uzma I. Zakai,[†] Shao-Zhong Zhang,[‡] Eric Block,^{*,‡} and Richard S. Glass^{*,†}

[†]Department of Chemistry, The University of Arizona, Tucson, Arizona 85721, [‡]Department of Chemistry, University at Albany, State University of New York, Albany, New York 12222, and [§]Department of Chemistry, Vanguard University, Costa Mesa, California 92626

evansd@purdue.edu; rglass@u.arizona.edu; eb801@albany.edu

Received January 13, 2010



The diverse electrochemical and chemical oxidations of dichalcogena-mesocycles are analyzed, broadening our understanding of the chemistry of the corresponding radical cations and dications. 1,5-Diselenocane and 1,5-ditellurocane undergo reversible two-electron oxidation with inverted potentials analogous to 1,5-dithiocane. On the other hand, 1,5-selenathiocane and 1,5-tellurathiocane undergo one-electron oxidative dimerization. The X-ray crystal structures of the Se–Se dimer of the 1,5-selenathiocane one-electron oxidized product and the monomeric two-electron oxidized product (dication) of 1,5-tellurathiocane are reported. 1,5-Dithiocanes and 1,5-diselenocanes with group 14 atoms as ring members undergo irreversible oxidation, unlike the reversible two-electron oxidation of the corresponding silicon-containing 1,5-ditellurocanes. These results demonstrate the chemical consequences of the dication stabilities $\text{Te}^+-\text{Te}^+ > \text{Se}^+-\text{Se}^+ > \text{S}^+-\text{S}^+$, as well as $\text{Se}^+-\text{Se}^+ > \text{Se}^+-\text{S}^+$ and $\text{Te}^+-\text{Te}^+ > \text{Te}^+-\text{S}^+$.

1. Introduction

The formation and reactions of sulfur radical cations have attracted considerable interest,¹ while far less attention has been given to the corresponding selenium and tellurium species.² Particular emphasis has been placed on uncovering the factors that affect the oxidation potential of the parent sulfur compound giving rise to the radical cation and the stability and fate of the radical cation or related species obtained by such oxidation. Such studies are relevant to

diverse areas such as electrically conducting materials³ and the pathogenesis of Alzheimer's disease.⁴

A seminal result in this area is the finding that chemical one-electron oxidation of 1,5-dithiocane (**1a**) produces a radical cation whose EPR spectrum persists for at least 72 h at room temperature.⁵ The remarkable persistence of this radical cation is ascribed to a transannular S–S bond,^{5,6} which is especially favorable in eight-membered rings due to the proximity of 1,5-positions and formation of two fused five-membered rings. Transannular interactions in eight-membered rings have long attracted interest, for example,

(1) Glass, R. S. *Top. Curr. Chem.* **1999**, *205*, 1–87.
(2) Detty, M. R.; Logan, M. E. *Adv. Phys. Org. Chem.* **2004**, *39*, 79–145.
(3) (a) Roncali, J. *Chem. Rev.* **1992**, *92*, 711–738. (b) Ishiguro, T.; Yamaji, K. *Organic Semiconductors*, 2nd ed.; Springer-Verlag: Berlin, Germany, 1998.
(c) *TTF Chemistry: Fundamentals and Applications of Tetrathiafulvalene*; Yamada, J., Sugimoto, T., Eds.; Kodansha-Springer: Hong Kong, 2004.
(d) Herranz, M. A.; Sanchez, L.; Martin, N. *Phosphorus, Sulfur Silicon Rel. Elem.* **2005**, *180*, 1133–1148. (e) Barbarella, G.; Melucci, M.; Sotgiu, G. *Adv. Mater.* **2005**, *17*, 1581–1593. (f) Roncali, J.; Blanchard, P.; Frere, P. *J. Mater. Chem.* **2005**, *15*, 1589–1610.

(4) (a) Varadarajan, S.; Yatin, S.; Kanski, J.; Jahanashahi, F.; Butterfield, D. A. *Brain Res. Bull.* **1999**, *50*, 133–141. (b) Butterfield, D. A.; Kanski, J. *Peptides* **2002**, *23*, 1299–1309. (c) Pogocki, D.; Schöneich, C. *Chem. Res. Toxicol.* **2002**, *15*, 408–418. (d) Schöneich, C.; Pogocki, D.; Hug, G. L.; Bobrowski, K. *J. Am. Chem. Soc.* **2003**, *125*, 13700–13713.

(5) Musker, W. K.; Wolford, T. L. *J. Am. Chem. Soc.* **1976**, *98*, 3055–3056.

(6) (a) Musker, W. K.; Wolford, T. L.; Roush, P. D. *J. Am. Chem. Soc.* **1978**, *100*, 6416–6421. (b) Musker, W. K. *Acc. Chem. Res.* **1980**, *13*, 200–206.

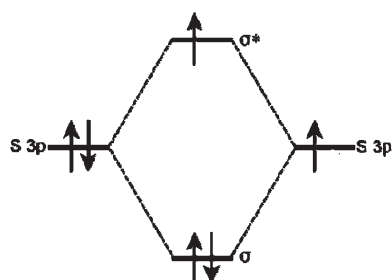
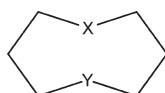


FIGURE 1. Simplified MO depiction of S,S 2c,3e bonding.

1,5-hydride shifts in cyclooctyl cations⁷ and transannular tertiary amine–carbonyl interactions.⁸ Electrochemical studies on **1a** have revealed three remarkable features: (1) its oxidation potential is 0.34 V (in CH₃CN vs Ag/0.1 M AgNO₃ in CH₃CN), which is almost 1 V less anodic than typical thioethers;⁹ (2) oxidation of **1a** is reversible, whereas typical thioethers undergo irreversible oxidation; and (3) the reversible oxidation peak for **1a** corresponds to a two-electron oxidation, which is ascribed to potential inversion—that is, **1a** undergoes two one-electron oxidations in which E° for the first step is more positive than that for the second step. All three features are attributed to neighboring group participation on oxidation, that is, transannular S–S bond formation lowering the oxidation potential. A 2c,3e S–S bond,¹⁰ depicted in Figure 1, is formed in which there is a σ^* -electron.

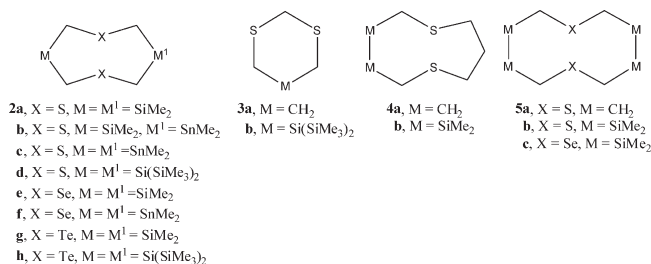


1a, X = Y = S; **b**, X = Y = Se; **c**, X = Y = Te
d, X = S, Y = Se; **e**, X = S, Y = Te; **f**, X = Se, Y = Te

Removal of this antibonding electron is favored electrochemically because S–S bonding is strengthened despite the electrostatic disfavoring of a dication relative to a monocation. Transannular bond formation also stabilizes the dication, which has also been chemically synthesized and structurally characterized by X-ray analysis.¹¹ The dication can be reduced before it undergoes chemical decomposition, resulting in reversible electrochemical behavior.

This paper reports the results of a systematic study of the redox properties of the selenium and tellurium analogues of

1,5-dithiocane **1a**, particularly **1d** and **1e** whose preparation we have recently described (compound **1f** remains unknown).¹² In addition, the redox properties of cyclic dichalcogenoethers with Si or Sn substituents **2–5** were studied electrochemically inspired by previous work.



That is, such Si and Sn substituents substantially lower the ionization energy of dichalcogenoethers in certain cases.¹³ However, chemical oxidation of these systems results in decomposition, especially ring cleavage.¹² Electrochemical studies provide a useful probe for discerning the competition between chalcogen–chalcogen bond formation stabilizing these systems and ring cleavage facilitated by Si or Sn.

Before presenting these results, a brief review of the work done by others on these and related compounds is warranted. Chemical oxidation of 1,5-diselenocane, **1b**, produced the corresponding dication with a transannular bond between the selenium atoms,^{14,15} which was characterized spectroscopically and by an X-ray crystallographic structure analysis of its BF₄ salt.¹⁶ Comproportionation of this dication with **1b** or one-electron oxidation of **1b** with NOPF₆ provided the corresponding radical cation as deduced from the appearance of an EPR signal.¹⁷ Cyclic voltammetric studies of this dication showed a reversible reduction peak in acetonitrile at an unusually low reduction potential of +0.11 V vs a Ag/0.01 M AgNO₃ in CH₃CN reference electrode.¹⁷ Analogous dications with a transannular Se–Se bond were obtained in 6- and 10-membered rings.¹⁴ Both radical cation and dication¹⁸ were formed by chemical oxidation of **6**. The dication was also produced by treatment of the corresponding selenoxide with concentrated H₂SO₄. Cyclic voltammetric studies of **6** in acetonitrile¹⁸ reveal a reversible oxidation peak at +0.33 V vs a Ag/0.01 M AgNO₃ in CH₃CN reference electrode. Chemical oxidation of **1c** provided the corresponding dication with a transannular Te–Te bond as deduced from ¹H, ¹³C, and ¹²⁵Te NMR spectroscopic studies.¹⁹ The cyclic voltammogram of **1c** showed one reversible

(7) Roberts, A. A.; Anderson, C. B. *Tetrahedron Lett.* **1969**, 3883–3885.

(8) (a) Leonard, N. J. *Rec. Chem. Prog.* **1956**, *17*, 243–257. (b) Leonard, N. J. *Acc. Chem. Res.* **1979**, *12*, 423–429. (c) Rademacher, P. *Chem. Soc. Rev.* **2002**, *24*, 143–150.

(9) (a) Wilson, G. S.; Swanson, D. D.; Klug, J. T.; Glass, R. S.; Ryan, M. D.; Musker, W. K. *J. Am. Chem. Soc.* **1979**, *101*, 1040–1042. (b) Ryan, M. D.; Swanson, D. D.; Glass, R. S.; Wilson, G. S. *J. Phys. Chem.* **1981**, *85*, 1069–1075.

(10) (a) Asmus, K.-D. *Acc. Chem. Res.* **1979**, *12*, 436–442. (b) Stowasser, R.; Glass, R. S.; Hoffmann, R. *J. Chem. Soc., Perkin Trans. 2* **1999**, 1559–1561. (c) Nakayama, N.; Takahashi, O.; Kikuchi, O.; Furukawa, N. *J. Mol. Struct. (Theochem)* **2001**, *542*, 215–226. (d) Maity, D. K. *J. Am. Chem. Soc.* **2002**, *124*, 8321–8328.

(11) (a) Iwasaki, F.; Toyoda, N.; Akaishi, R.; Fujihara, H.; Furukawa, N. *Bull. Chem. Soc. Jpn.* **1988**, *61*, 2563–2567. (b) Fujihara, H.; Kawada, A.; Furukawa, N. *J. Org. Chem.* **1987**, *52*, 4254–4257.

(12) (a) Block, E.; Dikarev, E. V.; Glass, R. S.; Jin, J.; Li, B.; Li, X.; Zhang, S.-Z. *J. Am. Chem. Soc.* **2006**, *128*, 14949–14961. (b) Block, E.; Glass, R. S.; Dikarev, E. V.; Gruhn, N. E.; Jin, J.; Li, B.; Lorange, E.; Zakai, U. I.; Zhang, S. Z. *Heteroat. Chem.* **2007**, *18*, 509–515. (c) Liao, C.; Zhang, S.-Z.; Block, E.; Clennan, E. L. *J. Org. Chem.* **2008**, *73*, 8587–8590.

(13) (a) Glass, R. S.; Block, E.; Lorange, E.; Zakai, U. I.; Gruhn, N. E.; Jin, J.; Zhang, S.-Z. *J. Am. Chem. Soc.* **2006**, *128*, 12685–12692. (b) Glass, R. S.; Block, E.; Gruhn, N. E.; Jin, J.; Lorange, E.; Zakai, U. I.; Zhang, S.-Z. *J. Org. Chem.* **2007**, *72*, 8290–8297.

(14) (a) Fujihara, H.; Akaishi, R.; Erata, T.; Furukawa, N. *Chem. Commun.* **1989**, 1789–1790. (b) Fujihara, H.; Akaishi, R.; Furukawa, N. *Tetrahedron* **1993**, *49*, 1605–1618.

(15) Batchelor, R. J.; Einstein, F. W. B.; Gay, I. D.; Gu, J.-H.; Mehta, S.; Pinto, B. M.; Zhou, X.-M. *Inorg. Chem.* **2000**, *39*, 2558–2571.

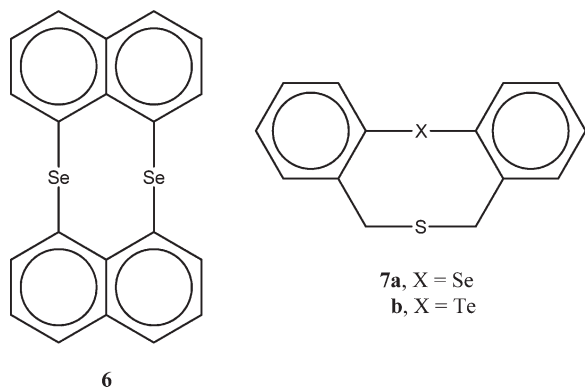
(16) (a) Iwasaki, F.; Morimoto, M.; Yasui, M.; Akaishi, R.; Fujihara, H.; Furukawa, N. *Acta Crystallogr.* **1991**, *C47*, 1463–1466. (b) Fujihara, H.; Furukawa, N. *Phosphorus, Sulfur Silicon Rel. Elem.* **1992**, *67*, 131–134.

(17) Fujihara, H.; Akaishi, R.; Nakamura, A.; Furukawa, N. *Tetrahedron Lett.* **1990**, *31*, 6375–6378.

(18) Fujihara, H.; Yabe, M.; Chiu, J.-J.; Furukawa, N. *Tetrahedron Lett.* **1991**, *32*, 4345–4348.

(19) Fujihara, H.; Ninoi, T.; Akaishi, R.; Erata, T.; Furukawa, N. *Tetrahedron Lett.* **1991**, *32*, 4537–4540.

oxidation peak at -0.02 V vs Ag/0.1 M AgNO₃. Related dihalogenoditelluranes were also reportedly formed by reaction of **1c** with iodine or chlorine.²⁰



Transannular interaction between S and Se, on the one hand, and S and Te, on the other, has been reported as well. Cyclic voltammetric studies on **7a** in acetonitrile showed a peak at a potential of $+0.75$ V vs a Ag/0.01 M AgNO₃ in CH₃CN reference electrode.²¹ Furthermore, chemical oxidation of **7a**, as well as treatment of the selenoxide of **7a** with sulfuric acid or triflic anhydride, gave the corresponding dication with a transannular Se–S bond as deduced from ¹H and ¹³C NMR spectroscopic studies.²¹ Cyclic voltammetric studies on **7b** in acetonitrile showed a peak at $+0.41$ V vs a Ag/0.01 M AgNO₃ in CH₃CN reference electrode.²² Chemical oxidation of **7b** produced the corresponding Te–Te bonded dication as deduced from ¹H, ¹³C, and ¹²⁵Te NMR spectroscopic studies. Ab initio molecular orbital calculations on the dications derived from **1a–f** with a transannular chalcogen–chalcogen bond were reported.²³

2. Results and Discussion

2.1. Compounds 1a–c. As expected based on previous work,^{17,19} **1b** and **1c** show reversible electrochemical oxidation in acetonitrile. To gain more insight into these redox processes, cyclic voltammograms for the compounds were measured under a range of scan rates. In addition, the electrochemical oxidation of **1a** was reinvestigated.

Figure 2 shows typical cyclic voltammograms for **1b** at three scan rates and two different concentrations. The initial positive-going sweep reveals a single peak whose height corresponds to an overall two-electron oxidation of **1b**. On the return sweep a single overall two-electron reduction peak is seen. In congruence with the earlier analysis of the voltammograms of **1a**, the oxidation is interpreted in terms of stepwise removal of two electrons, forming first the cation radical and then the dication. The individual formal potentials for these two processes, E°_1 and E°_2 , respectively, are quite similar causing the two separate peaks that are normally

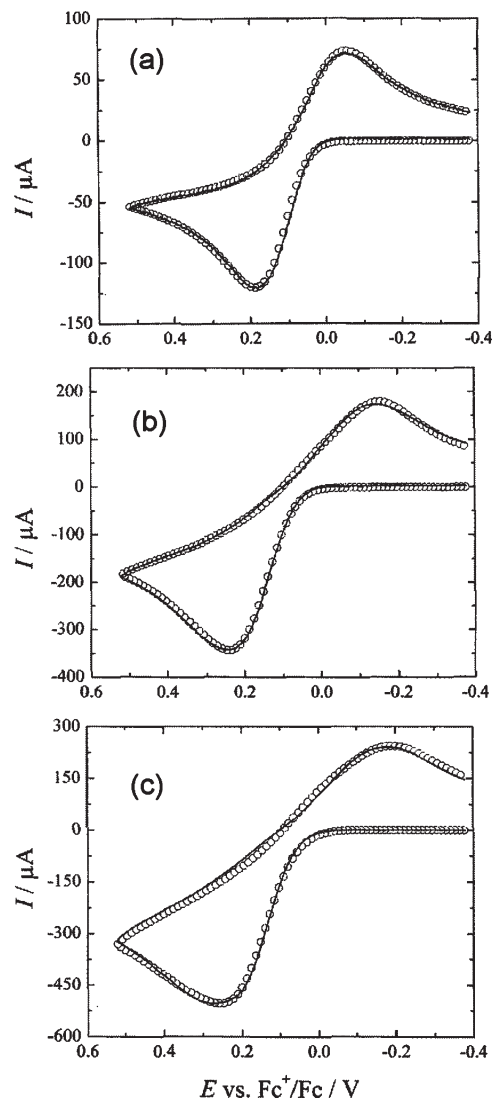


FIGURE 2. Cyclic voltammograms for **1b**: (a) 1.6 mM, 0.20 V/s; (b) 1.6 mM, 2.00 V/s; (c) 7.5 mM, 1.00 V/s, in 0.10 M NaClO₄/acetonitrile with use of a glassy carbon working electrode. The solid lines are the experimental results and the circles represent the theoretical simulation with the parameters listed in Table 1.

seen to overlap, forming a single two-electron oxidation peak. Similar arguments explain the single reduction peak that is seen. The shape of the voltammetric peaks for **1a** and **1c** was similar to those of **1b**.

In earlier work,^{9b} voltammograms of **1a** were interpreted in terms of an EE (electron transfer/electron transfer) process in which the individual formal potentials differed by only 20 mV and for which $E^{\circ}_1 - E^{\circ}_2$ was positive ($+20$ mV), which corresponds to “inverted potentials”.²⁴ This corresponds to the situation wherein the removal of the second electron from **1a** occurs with greater ease than removal of the first, although the difference was small in this case.

This potential inversion has previously been suggested to be a manifestation of the 2c,3e-bonding in [**1a**]²⁺. In this bonding scheme, shown in Figure 1, there are two electrons

(20) Fujihara, H.; Takaguchi, Y.; Ninoi, T.; Erata, T.; Furukawa, N. *J. Chem. Soc., Perkin Trans. 1* **1992**, 2583–2584.

(21) Fujihara, H.; Mima, H.; Chiu, J.-J.; Furukawa, N. *Tetrahedron Lett.* **1990**, 31, 2307–2310.

(22) Takaguchi, Y.; Fujihara, H.; Furukawa, N. *Organometallics* **1996**, 15, 1913–1919.

(23) (a) Fujihara, H.; Furukawa, N. *J. Mol. Struct. (Theochem)* **1989**, 186, 261–272. (b) Pissarev, S. A.; Shevchenko, N. E.; Nenaidenko, V. G.; Balenkova, E. S. *Russ. Chem. Bull. Int. Ed.* **2003**, 52, 1667–1673.

(24) For a recent example of potential inversion with numerous references, see: Macias-Ruvalcaba, N. A.; Evans, D. H. *J. Phys. Chem. B* **2006**, 110, 5155–5160.

TABLE 1. Parameter Values Found by Fitting Simulations to Voltammograms of Compounds **1a–c** and **2g,h** According to an EE Mechanism with Potential-Dependent Values of the Electron-Transfer Coefficient^a

compd	E°_1 , V	$k_{s,1}$, cm/s	λ_1 , eV	E°_2 , V	$k_{s,2}$, cm/s	λ_2 , eV	$E^{\circ}_{\text{overall}}$, V	$E^{\circ}_1 - E^{\circ}_2$, V
1a	0.404	0.025	– ^b	0.251	0.00051	0.30	0.327	0.153
1b	0.102	0.019	– ^b	0.058	0.012	0.45	0.080	0.044
1c	–0.294	0.0062	– ^b	–0.330	0.00085	0.17	–0.312	0.036
2g	–0.161	0.042	0.28	–0.372	0.031	0.057	–0.266	0.211
2h	–0.214	0.030	0.41	–0.237	0.0062	0.45	–0.226	0.023

^aPotentials are referred to the ferrocene/ferrocenium couple measured in acetonitrile. Concentrations were in the range of 0.5 to 4 mM in 0.10 M NaClO₄ in acetonitrile. For each compound voltammograms from 0.10 to 10 V/s were obtained and analyzed. Compound **1b** was studied at three concentrations (1.6, 4.0, and 7.5 mM). Diffusion coefficients were adjusted to match the anodic peak height and ranged from about 5×10^{-6} cm²/s for **2h** to 1.5×10^{-5} cm²/s for **1a**. Slight improvements in simulation of the voltammograms of **1a** and **1b** were obtained by including disproportionation ($2D^{+} \rightleftharpoons D + D^{2+}$) with disproportionation rate constants of 5.0×10^6 and 1.9×10^3 M^{–1}s^{–1}, respectively. Inclusion of disproportionation had no effect for **1c**, **2g,h**. For **2g** and **2h**, it was found that the simulated cathodic peak was larger than the experimental. This could be accounted for by inclusion of a slow decomposition reaction of the dication as was done previously for **1a**. However, addition of this reaction did not affect the electron-transfer parameters. ^bBest-fit values of λ_1 are large and correspond to the limit where α_1 changes negligibly over the potential range encompassed in the voltammogram. Specifically, $\Delta\alpha_1 \leq 0.05$. That is, for these compounds the electron-transfer kinetics of the first electron transfer follow the Butler–Volmer equations, eqs 1 and 2.

in the S–S σ molecular orbital and one in the antibonding σ^* molecular orbital. Consequently, removal of this antibonding electron on going from **[1a]^{•+}** to **[1a]²⁺** increases the S–S bond order, thus assisting the removal of the second electron. This is the qualitative basis for the potential inversion that is seen in **1a–c**.

In the earlier work,^{9b} the electron-transfer reactions were considered to follow the empirical Butler–Volmer formulation of heterogeneous electron-transfer kinetics.²⁵ Here, for the reaction of $CR + e^- \rightleftharpoons N$

$$k_{f,1} = k_{s,1} \exp \left[\frac{-\alpha_1 F}{RT} (E - E_1^{\circ}) \right] \quad (1)$$

$$k_{b,1} = k_{s,1} \exp \left[\frac{(1 - \alpha_1) F}{RT} (E - E_1^{\circ}) \right] \quad (2)$$

(where CR is the cation radical and N is the neutral species), the forward, k_f , and reverse, k_b , electron-transfer rate constants are given by eq 1 and 2. Here, $k_{s,1}$ is the standard heterogeneous electron-transfer rate constant, the rate constant when the potential, E , is equal to the formal potential, E°_1 , and α_1 is the electron-transfer coefficient. Both $k_{s,1}$ and α_1 are adjustable parameters used to fit the simulations to the experimental data, although α_1 is bounded by 0 and 1 and should be close to one-half. Analogous expressions are relevant for the second step of oxidation.

The previous simulations for **1a**, based on the Butler–Volmer formalism, provided fits that were approximately correct but which deviated in important details. In the present work we also found similar fits of simulation to experiment for **1a–c** when using these equations. The extent of agreement was definitely less than desired.

A conclusion derived from the Marcus theory of electron transfer²⁵ is that the electron-transfer coefficient is not a freely adjustable parameter but is given by eq 3. Here λ is the reorganization energy

$$\alpha = \frac{1}{2} + \left[\frac{E - E^{\circ}}{2\lambda} \right] \quad (3)$$

for the electron-transfer reaction. Equation 3 predicts that α is equal to one-half when the potential is equal to the

formal potential but that it will deviate from one-half as the potential is made either positive or negative of the formal potential. The key parameter here is the reorganization energy. Smaller values of λ cause a larger dependence of α on potential.

In the present case, we were able to obtain much improved fits of simulations with the experimental data using the potential-dependent α according to eq 3. These fits are illustrated by the points in Figure 2 (examples of fits of simulation with the voltammograms of **1c**, **2g**, and **2h** are shown in the Supporting Information). The parameters used are given in Table 1. The extent of potential inversion, $E^{\circ}_1 - E^{\circ}_2$, was found to be larger for **1a** than was found previously with the Butler–Volmer formulation. This difference in formal potentials is difficult to quantify in the case of potential inversion but we expect that the present result (+0.15 V) is more accurate than the earlier +0.02 V.

The overall potential for the two-electron reaction, E°_{ov} , which is given by $(E^{\circ}_1 + E^{\circ}_2)/2$, was found to be very similar for simulations based on Butler–Volmer and Marcus formulations although the extent of inversion differed significantly and, as mentioned above, the Marcus formulation provided better fits to the experimental voltammograms.

The lowest vertical ionization energies, IE, for **1a–c** have been determined by gas-phase photoelectron spectroscopy as 8.27,^{12b,26} 7.98,^{12b} and 7.59^{12b} eV, respectively. Their oxidation potentials, E°_1 , are +0.404, +0.102, and –0.294 V, respectively, and these provide an excellent linear correlation for this limited series ($E^{\circ}_1 = -8.081 + 1.026\text{IE}$; $R^2 = 0.9999$; slightly poorer correlation for E°_{ov} vs IE). The near-unity slope could mean that the solvation energies of the cation radicals of **1a–c** are almost constant, or that structural changes are compensating for differences in solvation energies. As will be seen below, such linear correlations of potential and ionization energy are not general nor are they expected to be general.^{27–29} The potential for the overall

(26) Setzer, W. N.; Coleman, B. R.; Wilson, G. S.; Glass, R. S. *Tetrahedron* **1981**, *37*, 2743–2747.

(27) Glass, R. S.; Andruski, S. W.; Broecker, J. L.; Firouzabadi, H.; Steffen, L. K.; Wilson, G. S. *J. Am. Chem. Soc.* **1989**, *111*, 4036–4045.

(28) Block, E.; Glass, R. S.; DeOrazio, R.; Lichtenberger, D. L.; Pollard, J. R.; Russell, E.; Schroeder, T. B.; Thiruvazhi, M.; Toscano, P. J. *Synlett* **1997**, 525–528.

(29) Block, E.; Birringer, M.; DeOrazio, R.; Fabian, J.; Glass, R. S.; Guo, C.; He, C.; Lorange, E.; Qian, Q.; Schroeder, T. B.; Shan, Z.; Thiruvazhi, M.; Wilson, G. S.; Zhang, X. *J. Am. Chem. Soc.* **2000**, *122*, 5052–5064.

(25) Bard, A. J.; Faulkner, L. R. *Electrochemical Methods. Fundamentals and Applications*, 2nd ed.; Wiley: New York, 2001; Sections 3.3, 3.4, and 3.6.

two-electron oxidation to the dications, E°_{ov} , represents the difference in energy between the dication and the corresponding neutral compound. Consequently, the order of stability of dication relative to the neutral compounds is $[\mathbf{1c}]^{2+} > [\mathbf{1b}]^{2+} > [\mathbf{1a}]^{2+}$. Enhanced stability of the dication relative to the neutral can be related both to relative atom ionization energies and the strength of the E–E bond in the dication. The order correlates very well with the relative atom ionization energies $\text{Te} < \text{Se} < \text{S}$,³⁰ but is reversed compared with chalcogen–chalcogen bond energies. It is well-known³¹ that the bond dissociation energy for chalcogen–chalcogen bonds follows the order $\text{S–S} > \text{Se–Se} > \text{Te–Te}$, i.e., Te–Te bonds are weaker than S–S or Se–Se bonds. Nevertheless, the values of E°_{ov} can reasonably be interpreted to mean that formation of a Te–Te bond is more favorable in $[\mathbf{1c}]^{2+}$ than a Se–Se bond in $[\mathbf{1b}]^{2+}$ or an S–S bond in $[\mathbf{1a}]^{2+}$. Indeed, ab initio calculations on 1,5-dichalcogenocanes^{32,33} show that the order of stability of the dications with respect to the neutral species is $[\mathbf{1c}]^{2+} > [\mathbf{1b}]^{2+} > [\mathbf{1a}]^{2+}$. In addition, the transannular bond order³⁴ between chalcogens increases on going from $[\text{S}_8]^{2+}$ to $[\text{Se}_8]^{2+}$ to $[\text{Te}_8]^{2+}$. Thus the reversal in bond strength from the usual $\text{S–S} > \text{Se–Se} > \text{Te–Te}$ to $\text{Te}^+–\text{Te}^+ > \text{Se}^+–\text{Se}^+ > \text{S}^+–\text{S}^+$ in dications is suggested to play a key role in explaining our results.

2.2. Compounds **1d and **1e**.** On the basis of the analysis presented above for **1a–c**, determination of the ionization energies for **1d** and **1e** might provide insight into their redox chemistry. Consequently the photoelectron spectra were measured for **1d** and **1e**, as shown in Figure 3. The lowest ionization energies for **1d** and **1e** are 8.11 and 7.73 eV, respectively. On the basis of the correlation of lowest vertical ionization energy and oxidation potentials reported above for **1a–c**, the oxidation potentials predicted for **1d** and **1e** are +0.240 and –0.054 V, respectively.

Interestingly, as seen in Figure 3, there is evidence for more than one conformer for **1d** and **1e**. To investigate this further, conformational analysis of **1d** and **1e** was carried out. On the basis of previous work³⁵ nine candidate conformations for the eight-membered ring were geometry optimized to obtain energy minima. Six conformations that are true energy minima and are within 4 kcal/mol of the lowest energy conformation were found for **1d** and seven for **1e**. Molecular orbital calculations were then done for each of these conformations and the two filled MOs of highest energy were plotted to aid in the analysis of their composition. For the

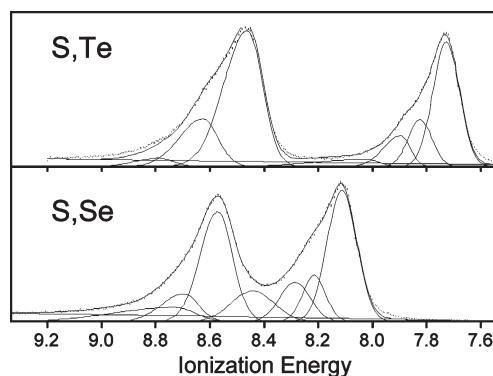


FIGURE 3. He I Photoelectron spectra of **1d** (lower) and **1e** (upper).

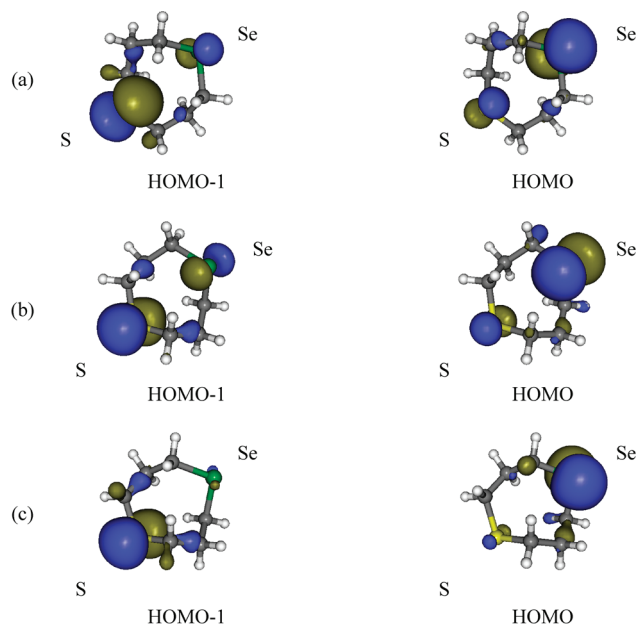


FIGURE 4. Three lowest energy conformations and plots of the HOMO and HOMO-1 for **1d**: (a) conformer B', (b) conformer B, and (c) conformer A.

three conformations of **1d** of lowest energy, plots of their two highest occupied MOs are shown in Figure 4. Plots of HOMO and HOMO-1 for the other conformations and the calculated relative energies of all of the conformers are given in the Supporting Information. For the four conformations of lowest energy of **1e**, plots of their two highest energy occupied MOs are shown in Figure 5. Plots of HOMO and HOMO-1 for all of the other conformations and the calculated relative energies of all of the conformers are given in the Supporting Information.

The results for HOMO and HOMO-1 for **1e** differ significantly from those of **1a**. The HOMO and HOMO-1 for **1a** are the symmetric and antisymmetric combinations of the p-type lone-pair orbitals on each of the transannular sulfur atoms. Similarly, HOMO and HOMO-1 for **1b** and **1c** are also the symmetric and antisymmetric p-type lone-pair orbitals on the selenium and tellurium atoms, respectively. However, for **1e** the HOMO is predominantly the 5p lone-pair orbital on Te and HOMO-1, the 3p lone-pair orbital on S. That is, there is no significant mixing of these lone-pair

(30) Chang, F. C.; Young, V. Y.; Prather, J. W.; Cheng, K. L. *J. Electron Spectrosc. Relat. Phenom.* **1986**, *40*, 363–383.

(31) (a) Pauling, L. *The Nature of the Chemical Bond*, 3rd ed.; Cornell University Press: Ithaca, NY, 1960, p 85. (b) www.chem.ox.ac.uk/icl/nometal-sold/lecture1/page11.html. (c) McDonough, J. E.; Weir, J. J.; Carlson, M. J.; Hoff, C. D.; Kryatova, O. P.; Rybak-Akimova, E. V.; Clough, C. R.; Cummins, C. C. *Inorg. Chem.* **2005**, *44*, 3127–3136.

(32) Nakayama, N.; Takahashi, O.; Kikuchi, O.; Furukawa, N. *Heteroat. Chem.* **2000**, *11*, 31–41.

(33) Selected calculations at the B3PW91/CEP-121G level correlate with the results at the RHF/3-21 G* level reported in ref 32. See Table S3 in the Supporting Information.

(34) Cameron, T. S.; Deeth, R. J.; Dionne, I.; Du, H.; Jenkins, H. D. B.; Krossing, I.; Passmore, J.; Roobottom, H. K. *Inorg. Chem.* **2000**, *39*, 5614–5631.

(35) (a) Clennan, E. L.; Hightower, S. E.; Greer, A. J. *Am. Chem. Soc.* **2005**, *127*, 11819–11826. (b) Laali, K.; Chen, H. Y.; Gerzins, R. J. *J. Org. Chem.* **1987**, *52*, 4126–4128. (c) Munson, E. J.; Kheir, A. A.; Haw, J. F. *J. Phys. Chem.* **1993**, *97*, 7321–7327. (d) Olah, G. A.; Svoboda, J. J.; Ku, A. T. *J. Org. Chem.* **1973**, *38*, 4447–4450.

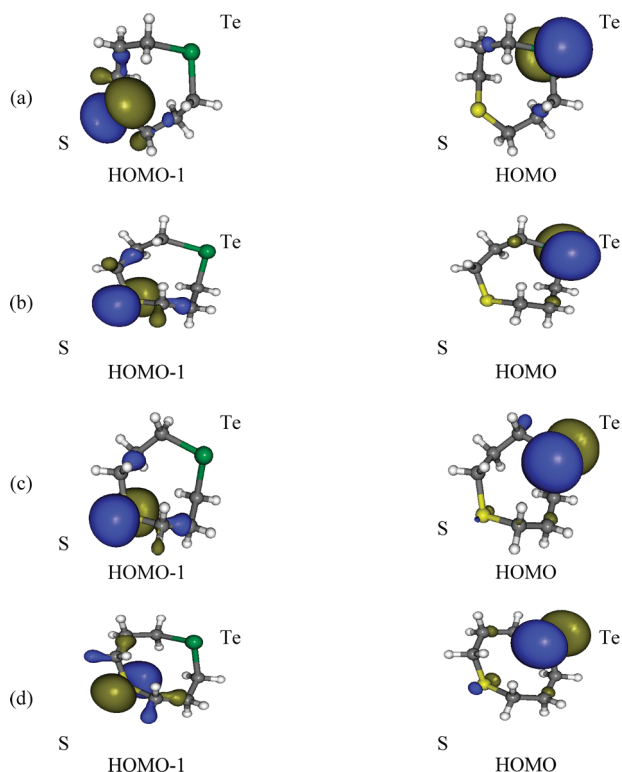


FIGURE 5. Four lowest energy conformations and plots of the HOMO and HOMO-1 for **1e**: (a) conformer B', (b) conformer A, (c) conformer B, and (d) conformer G.

orbitals. For **1d**, significant mixing of the 3p sulfur and 4p selenium lone-pair orbitals occurs in two of the lowest energy conformers (B' and B) but mixing is minimal in conformation A. These results are due to orbital energy differences and geometry effects on orbital overlap. This analysis supports the notion that the photoelectron spectra of **1d** and **1e** consist of ionizations from more than one conformation.

Furthermore, the corresponding dications from **1d** and **1e** were expected to be stable in view of reported ab initio calculations which showed that the order of stability of the dications with respect to the neutral species is $[\mathbf{1c}]^{2+} > [\mathbf{1b}]^{2+} > [\mathbf{1e}]^{2+} > [\mathbf{1d}]^{2+} > [\mathbf{1a}]^{2+}$.³² Chemical synthesis and characterization of salts of $[\mathbf{1d}]^{2+}$ and $[\mathbf{1e}]^{2+}$ is described below. These results led to the expectation that the electrochemical oxidation of **1d** and **1e** would be similar to that of **1a–c** in which the corresponding dications are reversibly formed at potentials reflective of their lowest ionization energies. However, the cyclic voltammetry results for **1d** and **1e**, run under the conditions outlined above for **1a–c**, diverge dramatically from those observed with the latter compounds. Figure 6 shows voltammograms of **1d** and **1e** obtained with differing scan rates. Rather than reversible oxidation to the corresponding dication, there are two steps of oxidation, both irreversible. As will be seen, the first corresponds to initial one-electron oxidation to form the cation radical, which in turn undergoes rapid dimerization to form a *dimer dication*. The second oxidation peak is due to the irreversible oxidation of this dimer dication. There is a single reduction peak, which is assigned to the reduction of the dimer dication to form the original neutral compound. The short-scan experiments include only the first oxidation and the reduction

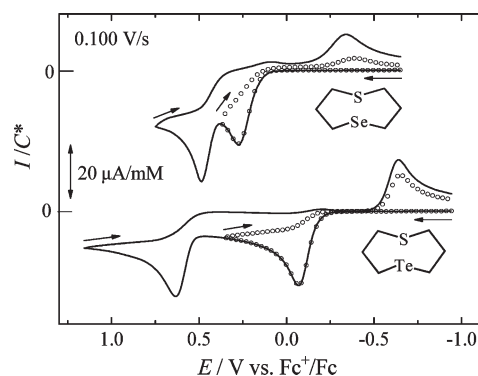


FIGURE 6. Cyclic voltammograms of **1d** and **1e** in acetonitrile with two different switching potentials (past first anodic peak: circles; past second anodic peak: full curves). The ordinate is the current divided by the concentration of **1d** or **1e**. Glassy carbon working electrode. **1d**: 5.6 mM; 0.10 M NBu₄PF₆. **1e**: 2.2 mM, 0.10 M NaClO₄.

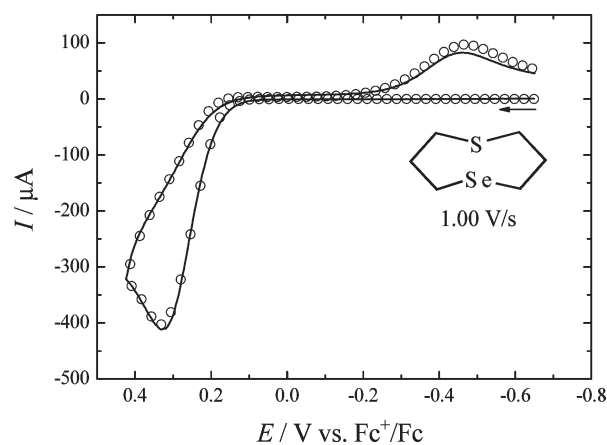
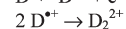
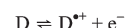


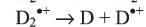
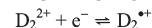
FIGURE 7. Comparison of background-corrected voltammogram of 5.5 mM **1d** (full curve) and simulation according to simulation parameter values listed in Table 2 (circles). Acetonitrile with 0.10 M NBu₄PF₆. Glassy carbon working electrode. Here 140 Ω of resistance was compensated in the experiment. The remaining 70 Ω was included in the simulation.

SCHEME 1^a

Initial Positive-going Scan:



Negative-going Return Scan:



^aD = **1d** or **1e**, D^{*+} is the corresponding cation radical, D₂²⁺ is the dimer dication, and D₂^{*+} is the dimer cation radical. Each electrode reaction has a standard potential, E^o, standard electron-transfer rate constant, k_s, and electron-transfer coefficient, α. Each chemical reaction has an equilibrium constant, K, forward rate constant, k_f, and reverse rate constant, k_b. Subscripts further identify the reaction. For example, K_{dim} is the equilibrium constant for dimerization and k_{r,dim} is the dimerization rate constant.

process and these have proven to be amenable to quantitative evaluation. The sulfur–tellurium compound is the more easily oxidized in the first step but this trend is reversed for the second oxidation peak.

TABLE 2. Values of Simulation Parameters for **1d** and **1e**^a

1-Selena-5-thiacyclooctane, 1d ^b			
electrode reactions	E°/V	$k_s / \text{cm s}^{-1}$	A
$D^{\bullet+} + e^- \rightleftharpoons D$	0.274	0.03	0.50
$D_2^{2+} + e^- \rightleftharpoons D_2^{\bullet+}$	-0.241	0.0010	0.40
$D_2^{4+} + 2e^- \rightleftharpoons D_2^{2+}$	0.269	0.000050	0.69
chemical reactions	K	k_f	k_b
$2 D^{\bullet+} \rightleftharpoons D_2^{2+}$	$5.0 \times 10^6 \text{ M}^{-1}$	$1.0 \times 10^6 \text{ M}^{-1} \text{ s}^{-1}$	0.20 s^{-1}
$D_2^{\bullet+} \rightleftharpoons D + D^{\bullet+}$	101 M^d	$1.0 \times 10^3 \text{ s}^{-1}$	$9.9 \text{ M}^{-1} \text{ s}^{-1}$
$D_2^{2+} \rightarrow \text{prod}$	irreversible	0.030 s^{-1}	n.a.
$D_2^{4+} \rightarrow \text{prod}'$	irreversible	100 s^{-1}	n.a.
1-Tellura-5-thiacyclooctane, 1e ^c			
electrode reactions	E°/V	$k_s / \text{cm s}^{-1}$	A
$D^{\bullet+} + e^- \rightleftharpoons D$	-0.054	0.03	0.50
$[D_2]^{2+} + e^- \rightleftharpoons D_2^{\bullet+}$	-0.724	0.05	0.50
chemical reactions	K	k_f	k_b
$2 D^{\bullet+} \rightleftharpoons D_2^{2+}$	$1.0 \times 10^8 \text{ M}^{-1}$	$1.0 \times 10^7 \text{ M}^{-1} \text{ s}^{-1}$	0.10 s^{-1}
$D_2^{\bullet+} \rightleftharpoons D + D^{\bullet+}$	$2.1 \times 10^3 \text{ M}^d$	$5.0 \times 10^4 \text{ s}^{-1}$	$24 \text{ M}^{-1} \text{ s}^{-1}$
$D_2^{2+} \rightarrow \text{prod}$	irreversible	0.010 s^{-1}	n.a.

^aData obtained in acetonitrile at a glassy carbon electrode. Potentials are referenced to ferrocene. For **1d** the diffusion coefficient of **1d** (and all other monomeric species in the mechanism) was set equal to $2.0 \times 10^{-5} \text{ cm}^2/\text{s}$ and $1.5 \times 10^{-5} \text{ cm}^2/\text{s}$ for dimeric species. For **1e** the values were $2.5 \times 10^{-5} \text{ cm}^2/\text{s}$ and $2.0 \times 10^{-5} \text{ cm}^2/\text{s}$, respectively. For compound **1d**, 140 Ω of solution resistance was electronically compensated and 70 Ω was included in the simulations. For compound **1e**, the values were 140 and 20 Ω . See Scheme 1 for definitions of the symbols used for the various species and definition of parameters. The choice of simulation parameter values for dimerization of the cation radicals is discussed in the text. The reaction $D_2^{\bullet+} \rightleftharpoons D + D^{\bullet+}$ was made to be fast and essentially irreversible in order to ensure that the overall reduction of D_2^{2+} had the stoichiometry $D_2^{2+} + 2e^- \rightarrow 2D$. This was found to produce good agreement between simulation and experiment for the reduction peak due to D_2^{2+} . For both compounds, a very slow irreversible decomposition of the dication dimer was found to provide an improvement in the fit of simulation to experiment. For **1d** the reaction $D_2^{4+} + 2e^- \rightleftharpoons D_2^{2+}$, coupled with rapid irreversible dissociation of D_2^{4+} , $D_2^{4+} \rightarrow \text{prod}'$, improves the fit on the positive-going sweep in the region following the anodic peak. This oxidation of the dimer dication can be seen in Figure 7. For **1e** the second step of oxidation is too far removed from the first to cause any appreciable additional current in this region. ^b0.10 M *n*-Bu₄NPF₆; 5.6 mM. ^c0.10 M NaClO₄; 2.2 mM. ^dValue dictated by $E^\circ_{D^{\bullet+}/D}$, $E^\circ_{D_2^{2+}/D_2^{\bullet+}}$, and K_{dim} .

A voltammogram of sulfur–selenium compound **1d** is shown in Figure 7. The oxidation peak occurs at about +0.4 V and its height corresponds to a one-electron process, which is thought to be oxidation to the cation radical followed by rapid dimerization to form the dimer dication (see Scheme 1). On the return sweep, the only feature is an irreversible reduction near -0.4 V, which is assigned to reduction of the dimer dication, proceeding in two steps to the original neutral molecule (Scheme 1).

The points in Figure 7 are for a simulation based on Scheme 1. At all of the scan rates employed (0.1 to 10 V/s), the initial oxidation is completely irreversible, signifying that the dimerization rate constant, $k_{f,\text{dim}}$, is large enough so that no peak for $D^{\bullet+} + e^- \rightarrow D$ is seen at the largest scan rate and K_{dim} is sufficiently large that no such peak is seen at the smallest scan rate (which would be seen if dimerization were significantly reversible). The values used in Figure 3, $K_{\text{dim}} = 5.0 \times 10^6 \text{ M}^{-1}$ and $k_{f,\text{dim}} = 1.0 \times 10^6 \text{ M}^{-1} \text{ s}^{-1}$, are not unique in their ability to account for the data, but they fall within a range of possible values corresponding to the lack of detection of a peak for reduction of the monomeric cation radical. The reduction peak near -0.4 V is accounted for by reduction of the dimer dication to an intermediate dimer cation radical followed by dissociation to the neutral molecule and the monomer cation radical, which in turn is reduced (Scheme 1). For a summary of all of the simulation parameters, see Table 2.

The same parameter values used in Figure 7 (listed in Table 2) were also found to provide reasonable agreement

between simulation and experiment for six other scan rates (0.1, 0.3, 0.5, 2, 3, 5 V/s). Comparison of simulations and experiments for these other scan rates are included in the Supporting Information.

These results are presaged by scattered earlier reports. One-electron oxidation of **1a** with NOPF₆ yielded a red diamagnetic solid, which was suggested to be the dimer of the radical cation of **1a**.⁶ On dissolution, it formed monomeric **1a**^{•+}. Electrochemical studies⁹ of **1a** revealed reversible dimerization of **[1a]**^{•+} in solution with $K_{\text{dim}} \approx 5000$ and a reduction potential for the dimer of -0.6 V. Ab initio calculations on the structure of this dimer suggested an intermolecular ⁺S–S⁺ bond stabilized by transannular S interactions, that is, a 4c, 6e-bond.³⁶ However, here we report the much more favorable dimerization of the radical cations of **1d** and **1e**, whose rates of dimerization and equilibrium constant are 3 orders of magnitude more favorable than those for the radical cation of **1a**. The consequences of these differences are dramatically reflected in the cyclic voltammograms under ordinary conditions in which **1a**, **1b**, and **1c** show a two-electron oxidation to the corresponding monomeric dication as discussed in Section 2.1 (albeit at high concentrations (2 mM), dimerization of **[1a]**^{•+} dominates over further oxidation to **[1a]**²⁺ so that an overall one, not two-electron, oxidation is observed for **1a**). In addition, these results reflect interesting differences in the behavior of

(36) Mantina, M.; Chamberlin, A. C.; Valero, R.; Cramer, C. J.; Truhlar, D. G. *J. Phys. Chem. A* **2009**, *113*, 5806–5812.

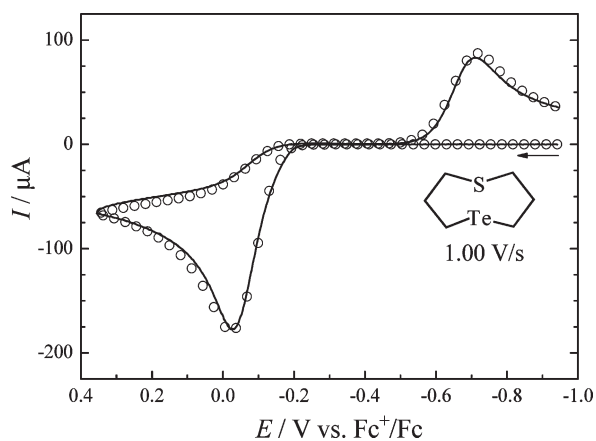


FIGURE 8. Comparison of background-corrected voltammogram of 2.2 mM **1e** (full curve) and simulation according to simulation parameter values listed in Table 2 (circles). Acetonitrile with 0.10 M NaClO₄. Glassy carbon working electrode. Here 140 Ω of resistance was compensated in the experiment. The remaining 20 Ω was included in the simulation.

the corresponding radical cations. Thus [**1a**]⁺ undergoes disproportionation to **1a** and [**1a**]²⁺ but the radical cations of **1d** and **1e** dimerize.

Controlled potential electrolysis of **1d** indicated that other reactions were occurring. For oxidation, the number of electrons per molecule exceeded 1.3 after 1700 s and the current had not approached zero at that time. However, cyclic voltammograms exhibited the reduction feature seen in Figure 7. Reductive electrolysis at a potential where the dimer dication was reduced recovered most of the charge and produced a solution whose voltammogram was almost identical with that from the original solution before the oxidation–reduction sequence. Thus, oxidation to the dimer dication followed by reduction back to the neutral roughly describes the stoichiometry of the reactions.

The results with the sulfur–tellurium compound, **1e**, were quite analogous to those seen for **1d**. An example of comparison of simulation with an experimental background-corrected voltammogram of **1e** is presented in Figure 8. The simulation parameters are included in Table 2 and comparisons of simulations with experiments for five other scan rates are included in the Supporting Information. In this case also, the values of K_{dim} and $k_{\text{f,dim}}$ were not uniquely determined but are consistent with a fast, essentially irreversible dimerization reaction.

Controlled potential electrolytic oxidation of **1e** proceeded smoothly and the current approached zero. However, only about one-half electron per molecule was required. The electrolyzed solution showed by cyclic voltammetry a peak for reduction of the dimer dication but about 0.1 V more negative than seen in voltammograms of neutral **1e**. Controlled potential reduction of this electrolyzed solution resulted in recovery of most of the charge. The only oxidation peak seen in the reduced solution was due to oxidation of **1e**, although its position was about 50 mV more positive than that seen in voltammograms of neutral **1e**. These results are essentially in agreement with the voltammetry and the differences are likely due to reactions that occur on the longer electrolysis time scale (> 2000 s) but are not important in the shorter cyclic voltammetry time scale (< ~20 s).

The key issue concerning the dimer dications [**D**]²⁺ obtained from **1d** and **1e** is their structure. Therefore chemical synthesis of these species was attempted. Oxidation of **1d** with tris(pentafluorophenyl)boron afforded the crystalline dimer [**(1d)**]₂²⁺[HOB(C₆F₅)₃]₂[−], whose structure was determined by X-ray methods. The molecular structure is shown in Figure 9. This is the first reported X-ray structure for a dimeric dication derived from 1,5-dichalcogenacyclooctanes. Each eight-membered ring adopts a BC conformation with the Se–Se bond occupying the equatorial position in each ring. The structure features an elongated Se–Se bond length of 2.641(1) Å (twice the covalent radius of Se is 2.25–2.45 Å; the Se–Se bond length in [**1b**]²⁺ is 2.382(2) Å) and S⋯Se distances of 2.830(3) Å, which is shorter than the sum of the van der Waals radii for S and Se (3.70 Å).³⁶ In addition, the S⋯Se⁺–Se⁺⋯S arrangement is almost linear. Consequently, this structure strongly resembles that calculated^{10c} for the most stable structure for [**(1a)**]₂²⁺, in which 4c, 6-bonding³⁷ in S⋯S⁺–S⁺⋯S was suggested. To be sure that [**(1d)**]₂²⁺ did not disproportionate in solution to **1d** and [**1d**]²⁺ its solution NMR spectrum was measured. To provide comparison NMR spectroscopic data for [**1d**]²⁺, this dication was synthesized by reaction of 5-thiaselenocane 5-oxide **8** (the thermodynamic product of peracid oxidation of **1d**; see Scheme 2)^{12c} with triflic anhydride at –50 °C, which gave [**1d**]₂²⁺[CF₃SO₃]₂[−] in essentially quantitative yield.

While the ¹H NMR spectra of the monomeric dications of **1a–c** have been reported to be complex, the 400 MHz ¹H NMR spectrum of [**1d**]₂²⁺[CF₃SO₃]₂[−] showed five well-defined multiplets centered at δ 4.30 (4H), 3.93 (2H), 3.80 (2H), 3.23 (2H), and 2.95 (2H). The ¹³C NMR spectrum showed three peaks at δ 52.1, 47.5, and 32.2 while the ⁷⁷Se NMR spectrum showed a single peak at δ 936. Through use of HMQC 2D NMR methods, the δ 52.1 ¹³C signal could be correlated with the δ 4.30 ¹H peak, the δ 47.5 ¹³C signal with the δ 3.93 and 3.80 peaks, and the ¹³C signal at δ 32.2 with the δ 3.23 and 2.95 peaks. Additional 2D NMR methods showed that the δ 4.30 peak was coupled to the δ 3.23 and 2.95 peaks but not to the δ 3.93 and 3.80 peaks; similarly, the tightly coupled multiplets at δ 3.93 and 3.80 were coupled to the δ 3.23 and 2.95 peaks but not to the 4.30 peak.

The structural assignment for [**1d**]₂²⁺[CF₃SO₃]₂[−] is consistent with several observations: (1) deshielding is seen in the ⁷⁷Se NMR peak (δ 936) compared to that seen in the starting material, 5-thiaselenocane 5-oxide (δ 156), and in model compounds Et₃Se⁺OTf (δ 373) and [**1b**]₂²⁺[PF₆]₂[−] (δ 806.5); (2) increasing shielding is seen in ¹³C and ¹H NMR spectra on going from related sulfonium to selenonium to telluronium ions (e.g., Me₃S⁺, δ 28 (¹³C) and 3.9 ppm (¹H); Me₃Se⁺ δ 22 (¹³C) and 2.7 ppm (¹H); Me₃Te⁺, δ 4 (¹³C) and 2.3 ppm (¹H)); (CH₃)₂(CH₃CH₂)S⁺, δ 38 (¹³C); (CH₃)₂(CH₃CH₂)Se⁺, δ 35.8 (¹³C); (CH₃)₂(CH₃CH₂)Te⁺, δ 18.2 (¹³C)).^{35b–d} On the basis of the above trends, the δ 52.1 ¹³C peak and the δ 4.30 ¹H peak, which is a triplet, are assigned to the methylene groups attached to sulfur while the 47.5 ¹³C peak and δ 3.93 and 3.80 ¹H peaks are assigned to the methylene group attached to selenium. The splitting pattern of the latter two sets of multiplets are quite similar to the ddd pattern seen for the CH₂S(O) protons in

(37) (a) Nakanishi, W.; Hayashi, S.; Toyota, S. *J. Org. Chem.* **1998**, *63*, 8790–8800. (b) Hayashi, S.; Nakanishi, W. *J. Org. Chem.* **1999**, *64*, 6688–6696. (c) Nakanishi, W.; Hayashi, S.; Morinaka, S.; Sasamori, T.; Tokitoh, N. *New J. Chem.* **2008**, *32*, 1881–1889.

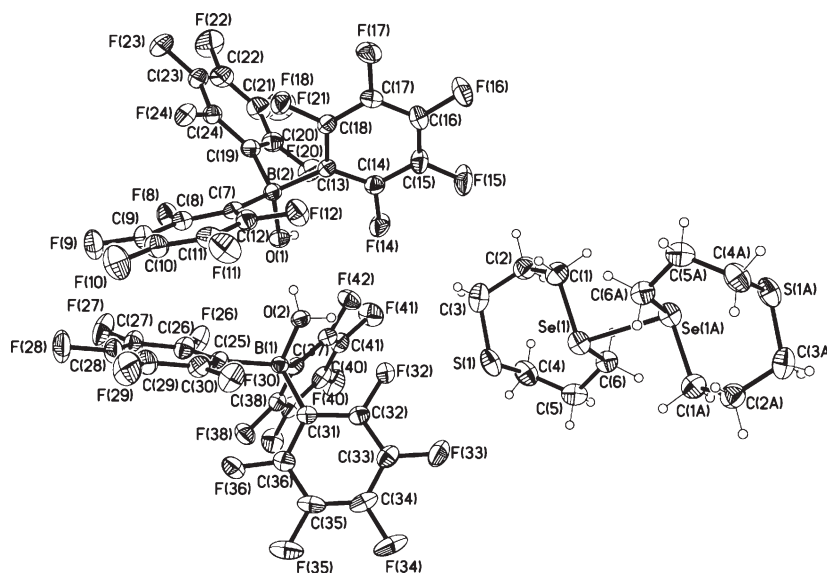
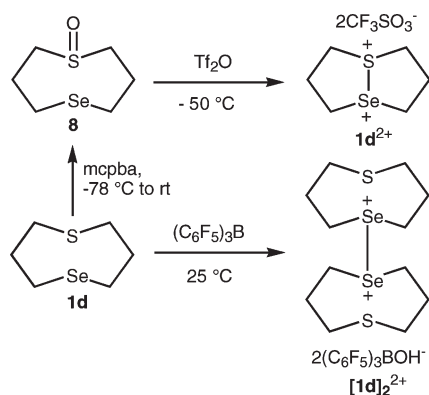


FIGURE 9. Drawing of $[\mathbf{1d}]_2^{2+}[\text{HOB}(\text{C}_6\text{F}_5)_3]_2$ based on X-ray crystallographic analysis. Se–Se 2.6471(6) Å, S···Se 2.830(3) Å; the S···Se⁺–Se⁺···S arrangement is almost linear; see the Supporting Information for further details.

SCHEME 2



5-thiaselenocane 5-oxide except that two of the central peaks overlap giving a seven-peak rather than eight-peak pattern. The coalescence of the diastereotopic methylene group protons adjacent to sulfur (giving a triplet rather than two eight-peak patterns) is similar to that seen for the methylene group protons adjacent to sulfur in the published ^1H NMR spectrum of $[\mathbf{1a}]^{2+}$, which appear as a singlet.^{11b}

The ^{77}Se NMR spectrum of the dimeric dication $[(\mathbf{1d})_2]^{2+}$ shows a peak at δ 867.3 ppm, which is different from that of $[\mathbf{1d}]^{2+}$ (936 ppm). The ^{77}Se NMR signal for $[(\mathbf{1d})_2]^{2+}$ is between that for $[\mathbf{1d}]^{2+}$ and that for $[\mathbf{1b}]^{2+}$ (806.5 ppm) supporting the existence of an $\text{Se}^+–\text{Se}^+$ moiety in the solution of $[(\mathbf{1d})_2]^{2+}$. Furthermore, the electrochemical studies with $[(\mathbf{1d})_2]^{2+}$ showed a reduction peak at -0.51 V just as observed in the cyclic voltammetric studies with $\mathbf{1d}$. Consequently the structure of the dimeric dication obtained electrochemically from $\mathbf{1d}$ can confidently be assigned to that shown in Scheme 2.

We were unsuccessful in converting $\mathbf{1e}$ in solution by chemical oxidation to a dimer similar to that prepared from $\mathbf{1d}$. Treatment of $\mathbf{1e}$ with tris(pentafluorophenyl)boron afforded crystalline 5-thiatellurocane 5-oxytris(pentafluorophenyl)boron $\text{S}[(\text{CH}_2)_3]_2\text{Te–O–B}(\text{C}_6\text{F}_5)_3$ ($\mathbf{9}$). In addition,

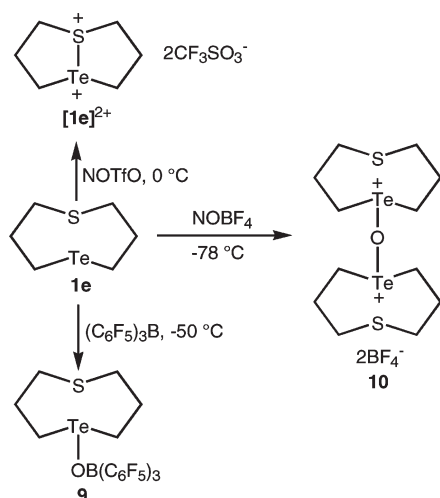
apparently due to the great sensitivity of the various oxidized tellurium species to oxygen, treatment of $\mathbf{1e}$ with NOBF_4 led to incorporation of oxygen giving the oxygen-bridged dimer $[\mathbf{1e–O–1e}]^{2+}[\text{BF}_4^-]_2$ ($\mathbf{10}$). Both structures were established by X-ray methods (see the Supporting Information for X-ray structures and experimental procedures which led to the two compounds). Insertion of an oxygen atom between tellurium atoms on oxidation of diaryl tellurides with NOBF_4 , or upon exposure of tellurium compounds to O_2 , has been previously reported.³⁸ These results are summarized in Scheme 3.

However, crystalline $[\mathbf{1e}]^{2+}[\text{CF}_3\text{SO}_3^-]_2$ could be obtained by oxidation of $\mathbf{1e}$ with nitrosonium triflate $[\text{NO}]^+[\text{CF}_3\text{SO}_3^-]$ at 0°C (Scheme 3). The structure of the dication could be determined by X-ray crystallographic analysis, as shown in Figure 10. The ^1H NMR spectrum of $[\mathbf{1e}]^{2+}[\text{CF}_3\text{SO}_3^-]_2$ shows six seven-peak multiplets, each with an enhanced central peak (3.94, 3.78, 3.51, 3.29, 3.04, 2.87); 2D NMR experiments show strong coupling of the 3.94/3.78 and 3.51/3.29 pairs, which are not coupled to each other, and presumably correspond to the methylene protons adjacent to sulfur and tellurium, respectively (see the Supporting Information for spectra). The ^{13}C NMR spectrum shows three peaks at δ 42.6, 39.1, and 29.3. The NMR spectra are quite similar in appearance to those described above for $[\mathbf{1d}]^{2+}[\text{CF}_3\text{SO}_3^-]_2$ except that both spectra are shifted slightly upfield and now the diastereotopic methylene protons on the carbon attached to sulfur appear as separate multiplets. Despite repeated attempts, the ^{125}Te NMR spectrum of $[\mathbf{1e}]^{2+}[\text{CF}_3\text{SO}_3^-]_2$ could not be obtained.

2.3. Compounds 2a–h, 3b, 4b, 5b, and 5c. Chemical oxidation of mixed sulfur-, selenium-, or tellurium-, and silicon- or tin-containing heterocycles has been reported elsewhere.¹² Electrochemical oxidation of these compounds, reported here, complements the chemical studies in several ways. Oxidation potentials provide quantitative information about the relative ease of oxidation and, if the oxidation is

(38) Kobayashi, K.; Deguchi, N.; Horn, E.; Furukawa, N. *Angew. Chem., Int. Ed.* **1998**, *37*, 984–986.

SCHEME 3



electrochemically reversible, then E° reflects the free energy differences between oxidized products and starting material. Reactive species produced by oxidation may be reduced before they decompose, especially when using cyclic voltammetry. Such studies may also provide mechanistic information as illustrated by cyclic voltammetric analysis as reported above.

It is known that the ionization energies and oxidation potentials of α -silylated thioethers³⁹ or selenides⁴⁰ are modestly lowered while those of α -stannylated thioethers⁴¹ are substantially lowered compared with those of the nonmetalated species. This lowering is geometry-dependent and greatest when the C–Si or C–Sn σ -orbitals are aligned with the sulfur or selenium p-type lone-pair orbitals.^{41a,c,42} Indeed, we reported elsewhere¹² that the ionization energies of **2a–h**, **3b**, **4b**, **5b**, and **5c** are lowered by this effect. The consequence of such lowering on the electrochemical oxidation potentials for these compounds is reported here. The electrochemical oxidation of these compounds is of further interest because, once the chalcogen is oxidized, it may be stabilized by transannular bond formation or undergo C–Si or C–Sn bond cleavage. In cases in which transannular bond formation is not an option, chalcogen radical cations formed either electrochemically, by photochemical electron transfer⁴³ or by one-electron metallic oxidants,⁴⁴ undergo

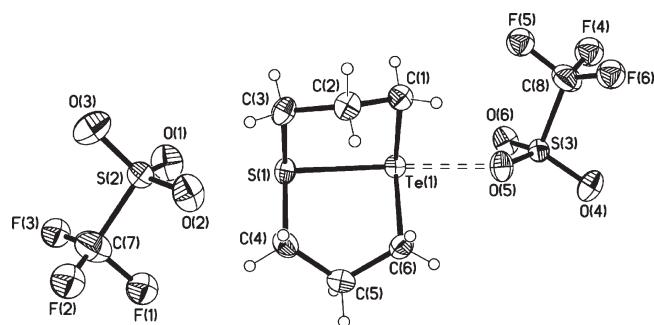
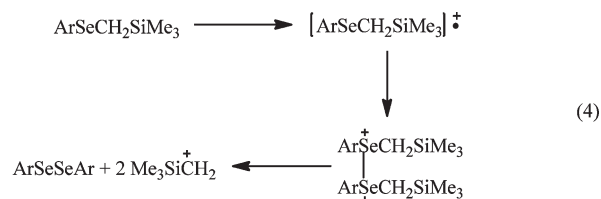


FIGURE 10. Drawing of $[1e]^{2+}(\text{CF}_3\text{SO}_3^-)_2$ based on X-ray crystallographic analysis.

selective cleavage of the C–Si or C–Sn bond.^{1,45} Such selective redox cleavages have been used to synthetic advantage. Electrochemical oxidation of aryl trimethylsilylmethyl selenides does not result in C–Si bond cleavage but rather an alternative cleavage pathway. The initially formed Se radical cation is suggested⁴⁰ to dimerize to an Se–Se bonded dication. This dication undergoes Se–C cleavage to afford diselenide and $\text{Me}_3\text{SiCH}_2^+$, as shown in eq 4. In addition, we have reported elsewhere¹³ that **2a**, **2e**, and **2g** on chemical oxidation undergo nucleophile-induced ring contraction.



Compounds **2a–e**, **3b**, **4b**, **5b**, and **5c** showed an irreversible oxidation and compound **2f** showed two irreversible oxidations at the peak potentials listed in Table 3. These oxidations were irreversible even at higher cyclic scan rates or in CH_2Cl_2 instead of CH_3CN as solvent. These irreversible oxidations contrast strongly with the previously reported reversible oxidations of **1a**⁹ and **1b**¹⁷ whose oxidation peak potentials are included in Table 3 for comparison. The irreversible oxidations seen for the first group suggest that either C–M bond cleavage or oxidative dimerization⁴⁰ is faster than transannular chalcogen–chalcogen bond formation on oxidation or that the oxidized species with a transannular chalcogen–chalcogen bond is kinetically unstable. The first process is analogous to the known cleavage of α -silylated and α -stannylated thioethers on one-electron oxidation.^{1,45} The second process is analogous to the known cleavage of aryl trimethylsilyl selenides on electrochemical oxidation (eq 4).³⁹ It should be noted that the HOMO ionization energies and electrochemical oxidation potentials do not correlate, unlike the situation with **1a–c**.⁴⁶ For example, consider the tellurium compounds **1c**, **2g**, and **2h**, in which **1c** has the highest ionization energy but least

(39) (a) Cooper, B. E.; Owen, W. J. *J. Organomet. Chem.* **1971**, *29*, 33–40. (b) Yoshida, J.; Isoe, S. *Chem. Lett.* **1987**, 631–634. (c) Block, E.; Yencha, A. J.; Aslam, M.; Eswarakrishnan, V.; Luo, J.; Sano, J. *J. Am. Chem. Soc.* **1988**, *110*, 4748–4753. (d) Block, E.; Aslam, M. *Tetrahedron* **1988**, *44*, 281–324. (e) Koizumi, T.; Fuchigami, T.; Nonaka, T. *Bull. Chem. Soc. Jpn.* **1989**, *62*, 219–225. (f) Yoshida, J.; Maekawa, T.; Murata, T.; Matsunaga, S.; Isoe, S. *J. Am. Chem. Soc.* **1990**, *112*, 1962–1970.

(40) Jouikov, V. V.; Fattakhova, D. S. *J. Organomet. Chem.* **2000**, *613*, 220–230.

(41) (a) Glass, R. S.; Radspinner, A. M.; Singh, W. P. *J. Am. Chem. Soc.* **1992**, *114*, 4921–4923. (b) Yoshida, J.; Ishichi, Y.; Nishiwaki, K.; Shiozawa, S.; Isoe, S. *Tetrahedron Lett.* **1992**, *33*, 2599–2602. (c) Glass, R. S.; Guo, Q.; Liu, Y. *Tetrahedron* **1997**, *53*, 12273–12286.

(42) Nishiwaki, K.; Yoshida, J. *Chem. Lett.* **1996**, 171–172.

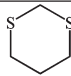
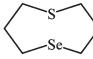
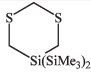
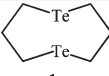
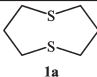
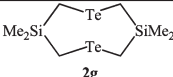
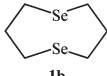
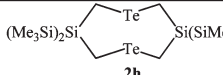
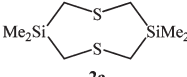
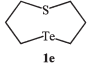
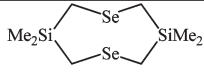
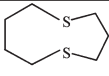
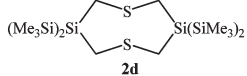
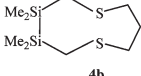
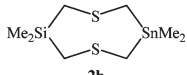
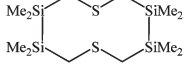
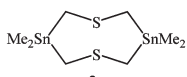
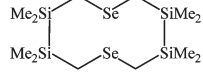
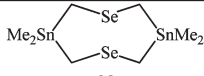
(43) (a) Hasegawa, E.; Brumfeld, M. A.; Mariano, P. S. *J. Org. Chem.* **1988**, *53*, 5435–5442. (b) Yoon, U.-C.; Kim, H.-J.; Mariano, P. S. *Heterocycles* **1989**, *29*, 1041. (c) Yoon, U. C.; Kim, U. C.; Choi, J. J.; Kim, D. U.; Mariano, P. S.; Cho, I.-S.; Jeon, Y. T. *J. Org. Chem.* **1992**, *57*, 1422–1428. (d) Ikeno, T.; Harada, M.; Arai, N.; Narasaka, K. *Chem. Lett.* **1997**, 169–170.

(44) (a) Narasaka, K.; Okauchi, T.; Arai, N. *Chem. Lett.* **1992**, 1229–1232. (b) Narasaka, K.; Arai, N.; Okauchi, T. *Bull. Chem. Soc. Jpn.* **1993**, *66*, 2995–3003.

(45) (a) Yoshida, J.; Nishiwaki, K. *J. Chem. Soc., Dalton Trans.* **1998**, 2589–2596. (b) Yoshida, J.; Kataoka, K.; Horcajada, R.; Nagaki, A. *Chem. Rev.* **2008**, *108*, 2265–2299.

(46) For example, those compounds that have oxidation peak potentials between 0.327 and 0.39 V (seven compounds: **1a**, **2a**, **2d**, **3a**, **3b**, **4a**, **4b**), a difference of only 60 mV, have first ionization energies varying substantially by 0.87 eV (7.51–8.38 eV). The λ_{max} of their charge transfer band correspondingly varies by 108 nm (520–628 nm).^{12b}

TABLE 3. Ionization Energies and Oxidation Potentials for Dichalcogena-Mesocycles

Compound	I.E., eV	E_p^a , V	Compound	I.E., eV	E_p^a , V
 3a	8.55, 8.44 ^b	0.656	 1d	8.11	0.277 (peak 1) 0.493 (peak 2)
 3b	7.80 ^c	1.11	 1c	7.59	-0.312 ^c
 1a	8.27 ^b	0.327 ^c	 2g	7.38	-0.266 ^c
 1b	8.00	0.080 ^c	 2h	7.04	-0.266 ^c
 2a	7.90	0.373	 1e	7.73	-0.063 (peak 1) 0.634 (peak 2)
 2e	7.71	0.218	 4a	8.36	0.39
 2d	7.51 ^d	0.338	 4b	7.85 ^c	0.386
 2b	7.59	0.312	 5b	7.61 ^c	0.515
 2c	7.50	0.206	 5c	7.45 ^c	0.367
 2f	7.60	-0.017 (peak 1) 0.785 (peak 2)			

^aPeak potentials (0.100 V/s) for irreversible oxidation. Potentials are referred to the reversible ferrocenium ion/ferrocene potential measured in acetonitrile. ^bReference 26. ^cReversible reactions with E° overall values taken from Table 1. ^dReference 13.

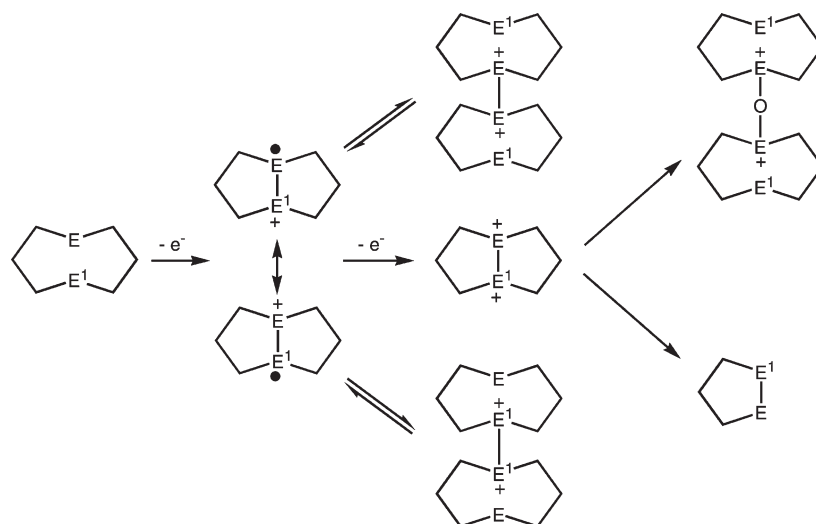
positive oxidation potential (albeit by only 60 mV) among the three. In principle, these need not correlate because the photoelectron spectroscopic measurement is a vertical, non-adiabatic process in the gas phase. On the other hand, the reversible electrochemical potentials reflect adiabatic ionization in solution containing supporting electrolyte.⁴⁷ Indeed lack of such correlation has been reported before.^{27–29} Also, there is an unknown and probably varying difference between the irreversible peak potential and the standard potential for

the first ionization of these compounds that will contribute to the lack of correlation.⁴⁷

In marked contrast to the sulfur compounds **2a–d** and selenium compounds **2e** and **2f**, tellurium compounds **2g** and **2h** showed reversible electrochemical oxidation as does 1,5-ditellurocane, **1c**. Clearly in these cases, the oxidized telluro compounds are stable and transannular Te–Te bond formation is faster than C–Si cleavage on oxidation. Although there may be several factors contributing to this result, we emphasize the key role played by transannular bond formation. The trend in bond strengths for dichalcogen dications discussed above is $\text{Te}^+ - \text{Te}^+ > \text{Se}^+ - \text{Se}^+ > \text{S}^+ - \text{S}^+$. Consequently,

(47) Glass, R. S.; Wilson, G. S.; Coleman, B. R.; Setzer, W. N.; Prabhu, U. D. G. *Adv. Chem. Ser.* **1982**, *201*, 417–441.

SCHEME 4



this trend in bond strength is proposed to account for the reversible electrochemical oxidation of **2g** and **2h** but irreversible electrochemical oxidation of **2a–f**.

3. Conclusions

The complex redox chemistry of 1,5-dichalcogenocanes and related compounds is summarized as shown in Scheme 4. The preferred pathway followed and stability of the products is predicated on the formation of the strongest dicationic bond, namely $\text{Te}^+-\text{Te}^+ > \text{Se}^+-\text{Se}^+ > \text{S}^+-\text{S}^+$, as well as $\text{Te}^+-\text{Te}^+ > \text{Te}^+-\text{S}^+$ and $\text{Se}^+-\text{Se}^+ > \text{Se}^+-\text{S}^+$. Furthermore, electrochemical oxidation under inert conditions and shorter time frame than chemical oxidations provides insight into intermediates that react with nucleophiles (or oxygen) under chemical oxidation conditions.

4. Experimental Section

General Methods. Anhydrous acetonitrile (AN, 99.8%, < 0.001% H_2O) was used as received and transferred via syringe under nitrogen. Sodium perchlorate was dried for 24 h in a vacuum oven at 70 °C. Tetrabutylammonium hexafluorophosphate (Bu_4NPF_6) was recrystallized three times from absolute ethanol and dried in a vacuum oven at 100 °C for 24 h before use. Compounds **1d** and **1e** were prepared as described elsewhere.¹² Tellurium compounds were manipulated in subdued light and were chromatographed with use of neutral alumina rather than silica gel, toward which they are unstable. Solvents were purified by standard procedures and were freshly distilled prior to use and deoxygenated with argon.

Cyclic Voltammetry. All electrochemical experiments were performed with either an EG&G Princeton Applied Research Potentiostat/Galvanostat, model 283, or a PARSTAT 2273, using a standard, jacketed three-electrode cell (10 mL). The experiments were conducted at room temperature (ca. 23 °C) in a nitrogen-inflated globe chamber (I^2R , model X-27-27) with the cell contents being purged with argon. The working electrode was a nominally 0.3-cm diameter glassy carbon electrode, while a platinum wire served as an auxiliary electrode and the reference electrode was an Ag/Ag^+ electrode (a silver wire immersed in 0.10 M $\text{Bu}_4\text{NPF}_6/0.01$ M silver nitrate/acetonitrile). The reference electrode was separated from the test solution by a porous Vycor frit. The potential of the silver reference electrode was periodically measured vs the potential of the ferrocenium/ferrocene couple in acetonitrile and all potentials are reported vs

ferrocene. The highly polished glassy carbon electrode was repolished before use and after each scan with 0.05- μm alumina paste, rinsed with water, and sonicated for 5 min in water. It was then rinsed with acetone and dried with a tissue. The areas of the two electrodes that were used were determined to be 0.0814 cm^2 and 0.0707 cm^2 based on simulations of voltammograms of known concentrations of ferrocene in acetonitrile at 298 K, using the consensus value of 2.5×10^{-5} cm^2/s for the diffusion coefficient of ferrocene.⁴⁸ The solution resistance, R_u , was almost completely compensated via IR compensation through positive feedback. The residual R_u was included in the simulations of the voltammograms.

Electrochemical Simulations. Digital simulations were conducted with DigiSim from Bioanalytical Systems, version 3.03, or DigiElch, version 2.0, a software package for the Digital simulation of common Electrochemical experiments (<http://www.elchsoft.com>).⁴⁹

Computational Methods. The various conformers of the various heterocycles were geometry optimized with B3LYP^{50,51}/CEP-121G⁵² and harmonic frequencies were determined. These frequencies assured that the conformers were genuine and provided free energies which in turn allowed the calculation of conformer populations.

Orbital energies were estimated both by (1) determining the ionization potential from the difference in radical cation electronic energy and neutral electronic energy at the geometry of the neutral (the ΔSCF method) and the HOMO/HOMO-1

(48) Hong, S. H.; Kraiya, C.; Lehmann, M. W.; Evans, D. H. *Anal. Chem.* **2000**, *72*, 454–458.

(49) Rudolph, M. *J. Electroanal. Chem.* **2003**, *543*, 23–29.

(50) As implemented in G03: Frisch, M. J., et al. *Gaussian 03*, Revision D.01; Gaussian, Inc., Wallingford, CT, 2004.

(51) (a) Becke, A. D. *J. Chem. Phys.* **1993**, *98*, 5648–5652. (b) Lee, C.; Yang, W.; Parr, R. G. *Phys. Rev. B* **1988**, *37*, 785–789. (c) Michlich, B.; Savin, A.; Stoll, H.; Preuss, H. *Chem. Phys. Lett.* **1989**, *157*, 200–206.

(52) Stevens, W. J.; Basch, H.; Krauss, M. *J. Chem. Phys.* **1984**, *81*, 6026–6033. Stevens, W. J.; Krauss, M.; Basch, H.; Jasien, P. G. *Can. J. Chem.* **1992**, *70*, 612–630. Cundari, T. R.; Stevens, W. J. *J. Chem. Phys.* **1993**, *98*, 5555–5565.

(53) Ortiz, J. V. *J. Chem. Phys.* **1988**, *89*, 6348–6352. Cederbaum, L. S. *J. Phys. (Paris)* **1975**, *B8*, 290–303. von Niessen, W.; Schirmer, J.; Cederbaum, L. S. *Comput. Phys. Rep.* **1984**, *1*, 57–125. Zakrzewski, V. G.; von Niessen, W. *J. Comput. Chem.* **1993**, *14*, 13–18. Zakrzewski, V. G.; Ortiz, J. V. *Int. J. Quantum Chem.* **1995**, *53*, 583–590. Ortiz, J. V. *Int. J. Quantum Chem. Symp.* **1988**, *34*, 431–436. Ortiz, J. V. *Int. J. Quantum Chem. Symp.* **1989**, *36*, 321–332. Ortiz, J. V.; Zakrzewski, V. G.; Dolgounircheva, O. In *Conceptual Perspectives in Quantum Chemistry*; Calais, J.-L., Kryachko E., Eds.; Kluwer Academic: New York, 1997; pp 465–518.

splitting from the Kohn–Sham orbital eigenvalues and (2) the Outer Valence Green's Function (OVGF)⁵³ method. The orbitals were visualized with use of Molekel.⁵⁴

The dications of the various heterocycles were also geometry optimized with B3LYP/CEP-121G and harmonic frequencies were determined; from this information, free energy differences were computed. Additionally, a Natural Bond Orbital (NBO) analysis⁵⁵ was conducted to determine the chalcogen–chalcogen bond occupancy.

Bond strength estimates for dichalcogen dications have been previously reported³² by computing the energy differences between the dication and neutral species, both in the chair–chair conformation. This was done at the RHF/3-21G* level. The same comparison was made by using the results of this study (at the B3PW91/CEP-121G level), but the **1a** neutral species was not computed in this study, and neither the neutral nor dication species of **1f** was computed in this study. Note that although the chalcogen atoms in the dications are formally hypervalent, neither the 3-21G* nor the CEP-121G basis set includes d-orbitals.

5-Thioniaseloniabicyclo[3.3.0]octane Bis(trifluoromethanesulfonate) ([1d]²⁺[CF₃SO₃][−])₂. To a solution of 5-thiaselenocane 5-oxide^{12c} (**8**; 15 mg, 0.07 mmol; NMR ¹H NMR (CDCl₃) δ 3.28–3.38 (m, 2H), 3.18–3.27 (m, 2H), 2.55–2.70 (m, 4H), 2.28–2.46 (m, 4H); ¹³C NMR (CDCl₃) δ 53.8, 24.3, 22.0; ⁷⁷Se (relative to Me₂Se) δ 156) in CD₃CN (0.6 mL) was added Tf₂O (20 mg, 0.07 mmol) at −50 °C and a colorless solution formed. The mixture was monitored by NMR at −50 °C and then at rt. The monomeric dication [1d]²⁺[CF₃SO₃][−]₂ was obtained in quantitative yield (by NMR); ¹H NMR (400 MHz, CD₃CN, rt) δ 4.30 (t, *J* = 6.4 Hz, 4 H), 3.93 (apparent ddd, 2 H), 3.80 (apparent ddd, 2 H), 3.23 (apparent dtt, 2 H), 2.95 (apparent dtt, 2 H); ¹³C NMR (CD₃CN) δ 52.1, 47.5, 32.2; ⁷⁷Se (relative to Me₂Se) δ 936. Crystals suitable for X-ray analysis could not be obtained. For the ¹H NMR spectrum see the Supporting Information.

5-Thioniatelluroniabicyclo[3.3.0]octane Bis(trifluoromethanesulfonate) ([1e]²⁺[CF₃SO₃][−])₂. To an ice-cooled solution of TfOH (97 mg, 0.64 mmol) in CH₃CN (5 mL) was added sodium nitrite (14.6 mg, 0.21 mmol). The mixture was stirred at 0 °C for 20 min, and then a solution of 5-thiatellurocane¹² (**1e**; 52 mg, 0.21 mmol; NMR ¹H NMR (400 MHz; CDCl₃) δ 2.93 (t, *J* = 6.0 Hz, 4 H), 2.74 (t, *J* = 6.0 Hz, 4 H), 2.24 (quin, *J* = 6.0 Hz, 4 H); ¹³C NMR (100 MHz) δ 32.7 (SC), 30.9 (CCC), 0.71 (TeC); ¹²⁵Te NMR δ 254 (relative to Me₂Te) in CH₃CN/CH₂Cl₂ (6 mL 1/1)

(54) Molekel 5.2.0.5; Swiss National Supercomputing Centre, Manno, Switzerland.

(55) Carpenter, J. E.; Weinhold, F. *J. Mol. Struct. (Theochem)* **1988**, *169*, 41–62. Carpenter, J. E., Ph.D. Thesis, University of Wisconsin, Madison, WI, **1987**. Foster, J. P.; Weinhold, F. *J. Am. Chem. Soc.* **1980**, *102*, 7211–7218. Reed, A. E.; Weinhold, F. *J. Chem. Phys.* **1983**, *78*, 4066–4073. Reed, A. E.; Weinhold, F. *J. Chem. Phys.* **1985**, *83*, 1736–1740. Reed, A. E.; Weinstock, R. B.; Weinhold, F. *J. Chem. Phys.* **1985**, *83*, 735–746. Reed, A. E.; Curtiss, L. A.; Weinhold, F. *Chem. Rev.* **1988**, *88*, 899–926. Weinhold, F.; Carpenter, J. E. In *The Structure of Small Molecules*; Naaman R., Vager, Z., Eds.; Plenum: New York, 1988; p 227.

was added to the above solution of NOTfO dropwise with stirring at 0 °C giving a pale yellow solution. The solution was kept at room temperature and the solvent was slowly evaporated whereupon crystals of [1e]²⁺[CF₃SO₃][−]₂ formed; mp 152–154 °C dec; ¹H NMR (CD₃CN, rt) δ 3.89–3.98 (m, 2 H), 3.74–3.83 (m, 2 H), 3.46–3.55 (m, 2 H), 3.25–3.34 (m, 2 H), 3.00–3.15 (m, 2 H), 2.80–2.93 (m, 2 H); ¹³C NMR (CD₃CN) δ 42.6, 39.1, 29.3. The ¹²⁵Te NMR spectrum could not be determined. The X-ray structure was determined and is shown in Figure 9 (see the Supporting Information for further details).

1,1'-Bis-5-thio-1-selenocanium Bis(B-hydroxytris(pentafluorophenyl)boron [1d]₂²⁺[HOB(C₆F₅)₃][−])₂. To a solution of 5-thiaselenocane¹² (**1d**; 12 mg, 0.06 mmol; NMR ¹H NMR (CDCl₃) δ 2.86 (t, *J* = 5.8 Hz, 4 H), 2.77 (t, *J* = 5.9 Hz, 4 H), 2.14 (quintet, *J* = 5.8 Hz, 4 H); ¹³C NMR (CDCl₃) δ 31.0, 30.8, 22.1; ⁷⁷Se NMR δ 164.6 (relative to Me₂Se) in CDCl₃ (0.6 mL) in an NMR tube was added solid B(C₆F₅)₃ (31.5 mg, 0.06 mmol) at room temperature. The solution was kept at rt for 4–5 days whereupon a small amount of orange crystals of the title compound was obtained, mp 158–159 °C dec; ¹H NMR (400 MHz, CD₃CN) δ 2.95–3.06 (m, 4 H), 2.73–2.86 (m, 4 H), 2.10–2.20 (m, 4 H); ¹³C NMR δ 150.1, 147.7, 139.1, 136.6, 32.1, 30.6, 27.5; ⁷⁷Se NMR (CD₃CN) δ 867.3 ppm (relative to Me₂Se). The X-ray structure was determined and is shown in Figure 10 (see the Supporting Information for further details).

Acknowledgment. The authors gratefully acknowledge support of this work by the donors of the Petroleum Research Fund, administered by the American Chemical Society (RSG, EB), and the National Science Foundation (CHE-0201555, CHE-0455575, RSG; CHE-9906566, CHE-0342660, CHE-0450505, CHE-0744578, EB; CHE-0347471, CHE-0715375, DHE).

Supporting Information Available: Comparison of simulations and background-corrected voltammograms for **1c**, **2g**, and **2h**, plots of HOMO and HOMO-1 of the other conformations of **1d** and **1e**, and tables of the absolute and calculated relative energies and their atomic coordinates of all of the conformers of **1d** and **1e**, comparison of selected calculated chalcogen–chalcogen bond stability with previous work, comparison of the simulations and background-corrected voltammograms for **1d** and **1e** at several scan rates, crystal data, and structure refinement for [1e]²⁺[(CF₃SO₃][−])₂ and [1d]₂[HOB(C₆F₅)₃][−]₂, experimental procedures as well as crystal data and structure refinement for 5-thiatellurocane 5-oxytris(pentafluorophenyl)boron (**8**), and 5,5'-oxy-bis(5-thiatellurocane) bis(tetrafluoroborate), (**9**), ¹H and ¹³C NMR spectra for [1d]²⁺[CF₃SO₃][−]₂, [1e]²⁺[CF₃SO₃][−]₂, **9**, and **10**, as well as a 2D ¹H–¹H spectrum for the latter, CIF files for the X-ray analysis for [(1d)₂]²⁺[HOB(C₆F₅)₃][−]₂, [1e]²⁺[CF₃SO₃][−]₂, **9**, and **10** (the crystal structure data has been deposited at the Cambridge Crystallographic Data Centre with deposition numbers 735750, 735753, 735751, and 735752, respectively), and full ref 50. This material is available free of charge via the Internet at <http://pubs.acs.org>.